Homogeneous Freezing of Concentrated Aqueous Nitric Acid Solutions at Polar Stratospheric Temperatures†

Dara Salcedo, Luisa T. Molina, and Mario J. Molina*

Department of Chemistry, and Earth, Atmospheric, and Planetary Sciences Department, Massachusetts Institute of Technology, Cambridge, Massachusetts 02139

Received: May 1, 2000; In Final Form: September 12, 2000

The freezing behavior of aqueous nitric acid solutions was investigated in order to elucidate the formation mechanism of solid polar stratospheric clouds (PSCs). Drops with composition ranging from 40 to 60 wt % HNO_3 were prepared and their phase transitions were monitored with an optical microscope. Homogeneous nucleation rates of nitric acid dihydrate (J_{NAD}) and nitric acid trihydrate (J_{NAT}) at temperatures between 175 and 195 K were estimated from the data. Classical nucleation theory was used to parametrize the results into simple equations to calculate J_{NAT} and J_{NAD} for different temperatures and concentrations of the liquid. The nucleation rate of the nitric acid hydrates was found to depend predominantly on the saturation ratio of the liquid with respect to the solid: higher saturation ratios correspond to higher nucleation rates. Both NAD and NAT can preferentially nucleate in binary nitric acid solutions, depending on the temperature and the composition of the liquid; also, NAD appears to catalyze the nucleation of NAT below ∼183 K. The results suggest that the largest drops in a PSC will freeze homogeneously if the stratospheric temperature remains near 190 K for more than 1 day, forming mixed liquid−solid clouds. In addition, the results indicate that nonequilibrium quasi-binary nitric acid solutions will not freeze in the stratosphere unless the temperature drops below 180 K.

Introduction

Polar stratospheric clouds (PSCs) appear during the wintertime over both poles. They have an important effect on the stratospheric ozone concentration since they provide surfaces for heterogeneous reactions to occur. These reactions convert relatively inert species ($ClONO_2$ and HCl) into reactive species that efficiently destroy ozone. PSCs can also cause denitrification of the stratosphere by scavenging nitrogen-containing species. The magnitude of these effects depends on the composition and phase of the PSCs.[1]

Field measurements have uncovered two types of PSCs above the frost point: type Ia consists of solid particles, and type Ib consists of liquid particles.[2,3] Type Ib PSCs form when the background aerosol, which consists of concentrated sulfuric acid drops, absorbs water and nitric acid as the temperature decreases in the winter. At ∼190 K, type Ib clouds consist of supercooled aqueous mixtures of nitric and sulfuric acid (∼ 40 wt % HNO_3 and ∼ 4 wt % H_2SO_4).[4−6] The freezing mechanism of these liquid clouds, which leads to the formation of type Ia clouds, is not well-understood. Laboratory experiments have suggested that supercooled solutions in equilibrium with water and nitric acid vapors under stratospheric conditions will not freeze unless the temperature drops below the frost point.[7−9] Meilinger et al.[10] and Tsias et al.[11] proposed that rapid temperature fluctuations, such as those encountered in mountain lee waves, might cause ternary drops to depart from equilibrium and attain high concentrations of HNO_3 (52−58 wt %) and low concentrations of H_2SO_4 (<1 wt %), allowing freezing of the liquid drops. Aerosol-chamber experiments performed by Prenni et al.[12] support this theory. However, Bertram et al.[13] measured freezing temperatures of nitric acid/water particles using a flow tube technique and concluded that freezing of NAD in the atmosphere may be important only if rapid temperature fluctuations are larger than suggested by Meilinger et al. and Tsias et al.

The composition of type Ia clouds is also unclear. Nitric acid trihydrate (NAT) is the stable solid phase under stratospheric conditions. However, Worsnop et al.[14] proposed that metastable nitric acid dihydrate (NAD) is an important component of type Ia PSCs because it has a lower energy barrier for nucleation and can freeze preferentially. It is not clear whether NAD can transform into NAT under stratospheric conditions. Clearly, to quantify the effect of PSCs on polar ozone chemistry, more work needs to be done to understand the freezing behavior of nitric acid solutions under polar stratospheric conditions.

Recently, FTIR, calorimetry, and optical microscopy techniques have been developed in our laboratory to study the freezing behavior of small drops.[9,15,16] We have also presented a procedure to calculate nucleation rates in liquid drops from the experimental data and used this procedure to estimate nucleation rates of NAD in 1:2 HNO_3/H_2O solutions at stratospheric temperatures.[17] In this report we extend that work to measurements of NAT and NAD nucleation rates in nonstoichiometric binary nitric acid solutions. Also, we use classical nucleation theory to parametrize our results together with those from Bertram and Sloan.[18,19] Finally, we discuss the implications of the results for the formation mechanism of polar stratospheric clouds.

Experimental Technique

The experimental apparatus is similar to the one described previously[17] with minor modifications. Briefly, it consists of a temperature-controlled aluminum stage, on which the sample

† Part of the special issue "Harold Johnston Festschrift".

10.1021/jp001639s CCC: $20.00
Published on Web 11/03/2000

cell sits. The cell is made from a Teflon block (15 × 2.5 × 0.25 cm) with a 0.75-cm diameter hole in the center (particle chamber). To seal the chamber, glass slides are attached to the bottom and top with halocarbon grease. The bottom slide is treated with a commercially available organosilane (Prosil 28), which provides a hydrophobic surface layer. A flow system, built only with Teflon and stainless steel tubing and valves, is connected to the chamber. The temperature at the bottom of the chamber is measured with a platinum resistance thermometer located below the cell and can be controlled to a precision of 0.1 K at 273 K. The temperature reading was calibrated by measuring the melting point of water, *n*-dodecane, *n*-octane, and *n*-heptane; the maximum error was 1.0 K. The cooling block is coupled to a microscope (Zeiss Axioscope 20) equipped with a video camera and connected to a videotape recorder. Experimental conditions (time and temperature) were converted into a video signal, overlayed on the camera signal, and recorded simultaneously.

In a typical experiment, drops were prepared by condensing vapors of water and nitric acid on the bottom of the cold chamber and equilibrating them at 273.2 K with a solution of known composition. Subsequently, the cell was closed and the temperature lowered at a constant rate between 1 and 8 K min^{-1} either until all of the drops were frozen, or until no more freezing events were detected (usually to a value between 190 and 160 K). Finally, the temperature was raised again in order to determine the melting temperature of the frozen drops, and hence their composition. Freezing and melting of the drops were detected visually by changes in their morphology, and for every one of them, freezing and melting times and temperatures were recorded. Most of the drops froze in a fraction of a second while the temperature was lowered, indicating that the limiting step for freezing was the nucleation rate, rather than the crystal growth rate. Some drops took several seconds to completely freeze or did not show any sign of freezing during the cooling phase but froze when the temperature was raised. In these cases, the crystal growth rate was the limiting step in the freezing process, and hence, these drops were not taken into account in the calculation of the nucleation rates.

Between 30 and 60 drops with diameters between 15 and 85 μm were monitored in each experiment. The volume of the drops was estimated by multiplying the volume assuming spherical shape times a geometrical factor of 0.2, which we had previously determined experimentaly.[17] We estimate the total uncertainty in the calculated volumes to be 30%.

The homogeneous nucleation rates (the number of critical nuclei formed per unit time and volume) were calculated with the following equation

$$J = \frac{\omega\gamma}{V_{tot}\Delta T} \qquad (1)$$

where γ is the cooling rate, V_{tot} is the sum of the volume of all the liquid drops at the beginning of a temperature interval (ΔT = 0.5 K), and ω is the number of drops that freeze during ΔT. ω varied between 2 and 20. The 0.9 confidence intervals for J ranged from 40 to 150%, relative to the calculated value.

To derive eq 1, we assume that the liquid volume remains constant during the observation period corresponding to ΔT.[17] Hence, we discarded those intervals for which $V_f/V_{tot} > 0.2$ (V_f is the volume of the drops that freeze during ΔT). In almost all of the experiments, the first 5 or 10% of the drops froze a few degrees above the temperature at which most of the drops started freezing continuously, and control experiments with repeated cooling and warming indicated that the drops that froze first were often the same ones. Hence, the freezing of the first drops was probably triggered by impurities or surface defects on the slide. To avoid these heterogeneous effects, the first 10% of the drops that froze in each experiment were not considered in the calculations of J. We also discarded any drop that did not freeze within 5 min after the first freezing event to minimize mass transfer effects caused by the different vapor pressure of the solid and liquid drops.

TABLE 1: Summary of Experimental Results

wt % HNO_3 (HNO_3:H_2O)	no. of expts	% frozen drops	T_1 (K)[a] NAD drops	T_2 (K)[a] NAT drops	T_{NAD} (K)[b]	T_{NAT} (K)[b]
64 (~1:2)	8	100[c]	234		235.2	246.8
60 (1:2.3)	7	100[c]	232−234	251	234.4	251.8
57 (1:2.6)	5	100[c]	231−234	254	232.6	253.7
54 (~1:3)	1[e]	100[c]	228	255	229.8	254.3
	6	15−100[d]	224−228	254−255		
50 (1:3.5)	4	~15[c]		253	224.6	253.5
40 (1:5.3)	2	no freezing above 163 K				

[a] T_1 and T_2 are final melting temperatures of individual drops. [b] T_{NAD} and T_{NAT} are the expected melting temperatures of NAD and NAT. [c] All drops froze upon cooling in each experiments. [d] Some drops froze upon cooling and some upon warming. [e] This experiments is referred as 54-NAD in the text.

Results

The results of the freezing experiments are summarized in Table 1. We performed experiments with compositions of 60, 57, 54, 50, and 40 wt % HNO_3. For comparison purposes, we also present our previously reported experiments with 64 wt % HNO_3 solutions.[17]

The composition of the drops studied, the number of experiments performed for each composition, and the percent of drops that froze during each experiment are indicated in the first three columns. Among the 54 wt % HNO_3 experiments, the one with the largest drops (referred as 54-NAD) yielded different results than the rest, and therefore, it is treated separately.

The fourth and fifth columns in Table 1 show the final melting temperature of individual drops, which we classified as T_1 and T_2. Comparing T_1 and T_2 with the melting points of NAD (T_{NAD}, column 6) and NAT (T_{NAT}, column 7) we are able to identify the solid formed. T_1 corresponds to T_{NAD}; therefore, we will refer to the drops that melted at T_1 as "NAD drops". Similarly, those that melted at T_2 will be referred as "NAT drops", which probably include drops that contain only NAT as well as drops containing mixtures of NAD and NAT. In the mixed ones, NAD melts at the NAT−NAD eutectic temperature (T_{eu} = 232.4 K), but NAT remains until T_{NAT} is reached. In fact, some drops showed morphological changes close to T_{eu} but finally melted at T_{NAT}.

Figure 1 shows the percent of frozen NAT drops as a function of the minimum temperature reached in each experiment. This figure suggests that NAT formation is enhanced at $T < 183$ K and in the more diluted solutions.

Figure 2 shows the temperature at which 10% of the drops were frozen upon cooling ($T_{10\%}$) as a function of the average volume of the drops in each experiment ($V_{average}$). The scatter of the data in this figure is probably caused by heterogeneous freezing of the first couple of frozen drops. The slope of $T_{10\%}$ vs $V_{average}$ for the 50 and 54 wt % HNO_3 experiments seems to be different from the rest of the experiments. A possible reason is that most of these solutions froze below 175 K. At these temperatures, the viscosity of the solutions increases rapidly as

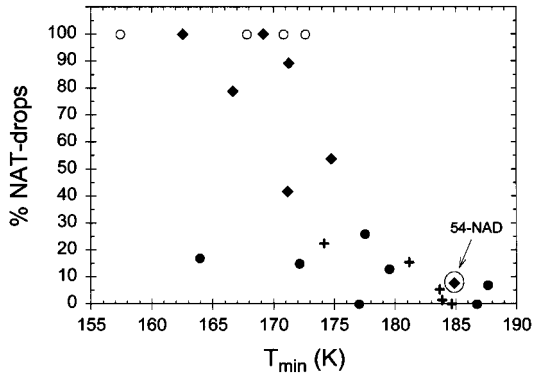

Figure 1. Percent of frozen drops containing NAT as a function of the minimum temperature reached in each experiment: (●) 60 wt % HNO_3, (+) 57 wt % HNO_3, (◆) 54 wt % HNO_3, (○) 50 wt % HNO_3.

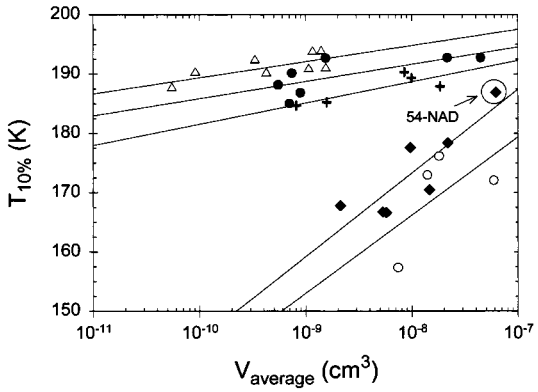

Figure 2. Temperature at which 10% of the drops were frozen as a function of the average volume of the drops in each experiment: (△) 64 wt % HNO_3,[17] (●) 60 wt % HNO_3, (+) 57 wt % HNO_3, (◆) 54 wt % HNO_3, (○) 50 wt % HNO_3. The lines are linear regression fits to each data set.

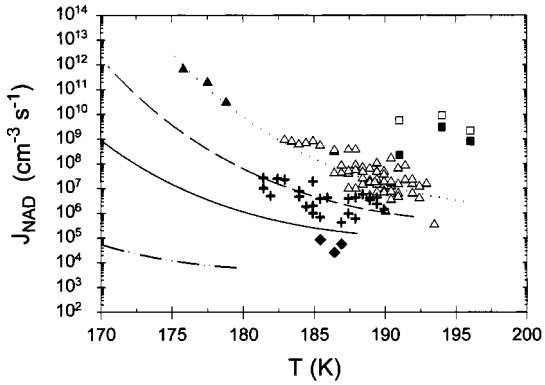

Figure 3. Nucleation rates of NAD as a function of temperature: (△) 64 wt % HNO_3,[17] (+) 57 wt % HNO_3, (◆) 54 wt % HNO_3, (▲) 63.4 wt % HNO_3,[18] (□) 63.4 wt % HNO_3,[12] and (■) 58.3 wt % HNO_3[12] The lines were calculated using eqs 2 and 7: (····) 64 wt % HNO_3, (− −) 57 wt % HNO_3, (—) 54 wt % HNO_3, (− ·· −) 50 wt % HNO_3.

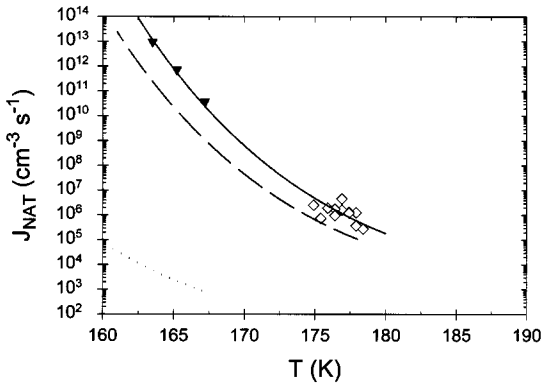

Figure 4. Nucleation rates of NAT as a function of temperature. (◇) 54 wt % HNO_3, (▼) 53.7 wt % HNO_3.[19] The lines were calculated using eqs 2 and 10: (—) 54 wt % HNO_3, (− −) 50% HNO_3, (····) 43 wt % HNO_3.

the temperature decreases, and the freezing rate becomes very slow; fewer drops would freeze under these conditions. Measurements by Tisdale et al.[20] support this explanation by showing that the viscosity of a 63.4 wt % HNO_3 solution increases 4 orders of magnitude from 170 to 160 K, while it only increases 2 orders of magnitude from 180 to 170 K.

According to Figure 2, the freezing temperature of the drops depends on their composition and volume. For drops with the same composition, the larger ones freeze at higher temperatures, because the probability that a nucleation event occurs is proportional to the volume of the liquid. On the other hand, for drops with the same size, the 64 wt % HNO_3 drops freeze at the highest temperatures, while the 40 wt % drops never freeze. This is a reflection of the decrease of the nucleation rate when the composition changes, as we will show below.

The nucleation rates for 60, 57, and 54 wt % HNO_3 solutions are calculated from the freezing observations. Experiments 54-NAD and those with 60 and 57 wt % HNO_3 yielded mostly NAD drops and we did not use the NAT drops in these experiments for the nucleation rate calculations; hence, the calculated nucleation rates correspond to NAD formation (J_{NAD}). Figure 3 shows our J_{NAD} values, together with those reported previously,[12,17,18] as a function of T. Results for 60 wt % HNO_3 are omitted for clarity, but on average the values fall between those for 64 and 57 wt %. Our results do not agree with those reported by Prenni et al.,[12] as discussed previously.[17]

Two of the experiments with 54 wt % HNO_3 drops yielded mostly NAT, and we assume that their nucleation rates (J_{NAT}) correspond to the formation of NAT (see the section Nucleation of NAT for the justification). The calculated J_{NAT} are plotted in Figure 4 as a function of T; also included are J_{NAT} values from Bertram and Sloan.[19] In both sets of data, J increases as the temperature decreases. We could not calculate nucleation rates for the rest of the experiments with 54 and 50 wt % HNO_3 drops, because only ∼15% of the drops froze upon cooling. For the 40 wt % HNO_3 solutions, which did not freeze under our experimental conditions, we have calculated an upper limit to the nucleation rate. Assuming a volume per drop of $\sim 10^{-7}$ cm^{-3} and cooling rates of ∼3 K min^{-1}, this upper limit is $\sim 10^5$ cm^{-3} s^{-1}.

Nucleation of NAD. The formation of a solid phase from the liquid state can be described by classical nucleation theory (CNT). In this model, the phase transition is initiated by fluctuations that lead to the appearance of small regions of the crystalline phase. If these regions are larger than some critical size, they will grow spontaneously. The nucleation rate (J) is the number of these critical-sized nuclei formed per unit volume and time. CNT describes the nucleation process using a kinetic approach, leading to the following equation[21]

$$J = n_{liq}\left(\frac{kT}{h}\right)\exp\left(\frac{-\Delta G_{act}}{kT}\right) \qquad (2)$$

where n_{liq} is the molecular concentration in the liquid (in this case, the molecular concentration of nitrate ions in solution), k and h are the Boltzman and Planck constants, T is the temperature, and ΔG_{act} is the nucleation activation energy, which

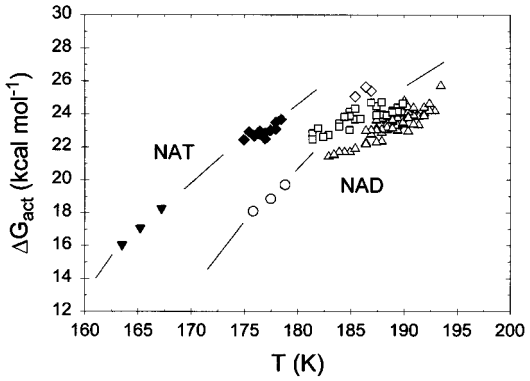

Figure 5. Nucleation activation energy as a function of temperature. Open symbols correspond to NAD: (△) 64 wt % HNO_3, (□) 57 wt % HNO_3, (◇) 54 wt % HNO_3, (○) 63.4 wt % HNO_3.[18] Closed symbols correspond to NAT: (◆) 54 wt % HNO_3, (▼) 53.7 wt % HNO_3.[19] The lines are for visual reference only.

has two components,

$$\Delta G_{act} = \Delta G^* + \Delta G_d \tag{3}$$

$$\Delta G^* = \frac{16\pi}{3}\sigma_{sl}^3\left[\frac{\upsilon_{NAX}}{kT\ln(S_{NAX})}\right]^2 \tag{4}$$

where ΔG^* is the activation energy for the formation of a critical nucleus, υ_{NAX} is the molecular volume of the solid NAX (NAD or NAT), σ_{sl} is the interfacial energy per unit area between the liquid and solid phases, and S_{NAX} is the saturation ratio of the liquid with respect to the solid. S_{NAX} is the ratio between the activity product of the ions and solvent in the liquid over their activity product in a solution saturated with the solid (K_S). To estimate S_{NAX}, we use the model of Carslaw et al.[22] to calculate the activity of the species in the liquid and K_S for NAT. To calculate K_S for NAD we used eq A9 in Massucci et al.[23] ΔG_d (usually known as the activation diffusion energy) is the activation energy related to the diffusion of one molecule from the bulk liquid to the solid and is a function of the viscosity of the liquid. As the temperature decreases, ΔG^* decreases, because S_{NAX} increases and σ_{sl} decreases as the liquid becomes more "solid-like". On the other hand, ΔG_d increases as the temperature decreases, because the higher viscosity of the liquid makes diffusion more difficult. Therefore, the nucleation rate is expected to have a maximum at some specific temperature. CNT describes the nucleation process in a relatively simple way but has the disadvantage that it involves quantities such as σ_{sl} and ΔG_d that cannot be estimated a priori,[21] and it is not clear how these parameters depend on the temperature or the saturation ratios.

Figure 3 shows that J_{NAD} increases as T decreases, but there is no maximum. This observation suggests that in the temperature and composition ranges studied, ΔG_d is small and ΔG^* determines the temperature dependence of the nucleation rate. We expect that ΔG_d will become more important as the temperature reaches the glass transition (~160 K).[20]

Using eq 2, ΔG_{act} can be estimated from the measured nucleation rate

$$\Delta G_{act} = -kT\ln\left(\frac{h}{kT}\frac{J}{n_{liq}}\right) \tag{5}$$

where n_{liq} is in mol·cm^{-3} and J corresponds to our experimental values of J_{NAD} and those from Bertram and Sloan.[18] Figure 5 shows a plot of ΔG_{act} as a function of temperature; for clarity,

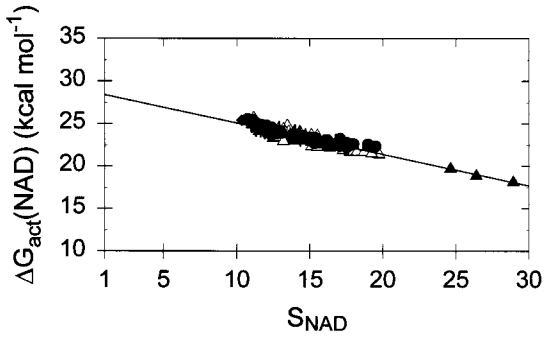

Figure 6. Nucleation activation energy of NAD as a function of the saturation ratio with respect to NAD: (△) 64 wt % HNO_3, (●) 60 wt % HNO_3, (+) 57 wt % HNO_3, (◆) 54 wt % HNO_3, (▲) 63.4 wt % HNO_3.[18] The solid line was calculated using eq 7.

ΔG_{act} for 60 wt % HNO_3 is not included, but on average it falls between the values for 64 and 57 wt % HNO_3. As expected, Figure 5 shows that at a given T the solutions with higher nucleation rate (the more concentrated ones) have lower energy barriers for nucleation.

Figure 6 shows a plot of ΔG_{act} for NAD versus S_{NAD}; in this case the data collapse into one single line (results for 60 wt % HNO_3 are also included in this figure); i.e., there is a linear relation between ΔG_{act} and S_{NAD} and it is the same for all liquid concentrations. We note that Figure 6 includes data obtained using two independent techniques, under different conditions of T and composition, yet all the data fall on the same line. We do not have an explanation for this linear relation. CNT is only of limited use in this respect, since the dependency of σ_{NAX} and υ_{NAX} on temperature and composition is unclear.

We parametrized the experimental J_{NAD} as a function of S_{NAD} by performing a linear regression fit to the data

$$\Delta G_{act} = (28.8 \pm 0.2) - (0.37 \pm 0.01)S_{NAD} \tag{7}$$

where ΔG_{act} is in kcal mol^{-1}. The correlation coefficient of the linear regression is $r = 0.93$. This equation is valid only for $10 < S_{NAD} < 30$, becasue our experimental data fall within this interval. Using eq 7 followed by eq 2, one can calculate J_{NAD} in HNO_3 solutions with different concentrations at different temperatures, as long as S_{NAD} is in the valid range. Curves calculated in this way for 64, 57, 54, and 50 wt % HNO_3 are plotted in Figure 3.

In an attempt to further facilitate the use of our results, we have calculated J_{NAD} using eqs 2 and 7 for nitric acid compositions between 50 and 64 wt % and from 170 to 200 K. The results obtained can be parametrized using the following equations

$$\ln J_{NAD} = A(0) + A(1)T + A(2)T^2 + A(3)T^3 + A(4)T^4 \tag{8}$$

$$A(i) = B_i(0) + B_i(1)w + B_i(2)w^2 + B_i(3)w^3 + B_i(4)w^4 \tag{9}$$

where w is the concentration of nitric acid in weight percent and coefficients $B_i(j)$ are given in Table 2. The maximum difference in J_{NAD} if eqs 8 and 9 are used instead of equations 2 and 7 is 5%.

Although we did not perform experiments with solutions more concentrated than 64 wt %, we can speculate that J_{NAD} has a maximum at 63.4 wt % HNO_3 (the stoichiometric composition for NAD), because this solution has the maximum saturation ratio at any given temperature. Hence, J_{NAD} should decrease in more concentrated solutions. This is in accordance with experiments by Bertram et al.,[13] who found that the maximum freezing

TABLE 2: Coefficients for Eq 9 to Calculate Nucleation Rates of NAD

$i=$	0	1	2	3	4
$B_i(0)$	10 945 616.89	−234 214.939 24	1 880.299 602 1	−6.711 414 523 5	$8.985\,811\,625 \times 10^{-3}$
$B_i(1)$	−781 356.449 85	16 745.051 036	−134.608 401 54	0.481 010 163 03	$-6.446\,481\,675\,8 \times 10^{-4}$
$B_i(2)$	20 791.740 99	−446.415 166 46	3.594 418 174 6	−0.012 862 469 834	$1.725\,951\,771 \times 10^{-5}$
$B_i(3)$	−244.280 265 67	5.256 274 529 9	−0.042 401 854 878	$1.519\,829\,456\,5 \times 10^{-4}$	$-2.042\,332\,859\,3 \times 10^{-7}$
$B_i(4)$	1.070 082 528	−0.023 079 581 7	$1.865\,602\,733 \times 10^{-4}$	$-6.698\,881\,44 \times 10^{-7}$	$9.016\,014\,451 \times 10^{-10}$

TABLE 3: Coefficients for Eq 12 to Calculate Nucleation Rates of NAT

$i=$	0	1	2	3	4
$E_i(0)$	14 917 832.065	−347 829.469 43	3 043.506 491	−11.843 155 128	0.017 291 414 1
$E_i(1)$	−1 242 036.231 2	28 981.349 854	−253.734 745 41	0.987 792 980 4	$-1.442\,674\,573\,5 \times 10^{-3}$
$E_i(2)$	38 606.210 85	−901.792 025 39	7.902 153 669 5	$-3.078\,481\,584\,3 \times 10^{-2}$	$4.498\,649\,441\,2 \times 10^{-5}$
$E_i(3)$	−530.506 009 68	12.409 113 21	−0.108 861 954 6	$4.245\,003\,029\,3 \times 10^{-4}$	$-6.208\,162\,434\,9 \times 10^{-7}$
$E_i(4)$	2.720 772 087 2	−0.063 743 579 7	$5.599\,487\,857\,3 \times 10^{-4}$	$-2.185\,910\,865\,5 \times 10^{-6}$	$3.199\,796\,61 \times 10^{-9}$

temperature of submicron-sized aerosols is at the stoichiometric concentration of NAD.

In recent studies of ice nucleation, critical nucleation parameters have been measured (temperature, concentration of the liquid, saturation ratio, water activity in solution, and supercooling).[15,24] These parameters mark a threshold for freezing: if it is crossed, ice will form, independently of the cooling rate or the volume of the sample. Although this is a very convenient approximation, it cannot be applied to NAD. The nucleation rate of ice has a large slope when plotted against temperature and the nucleation rate changes several orders of magnitude within a few degrees;[25] thus, the freezing temperature of samples with different volumes will be very similar. In contrast, J_{NAD} does not increase as fast when T decreases, and samples of different sizes freeze at temperatures several degrees apart.

Nucleation of NAT. It has been suggested that the homogeneous nucleation activation energy for NAT is large, and thus, it can only nucleate heterogeneously on the surface of previously formed NAD,[13,14,26] in contrast to our conclusion that NAT nucleates homogeneously in the 54 and 50 wt % HNO_3 drops (except in experiment 54-NAD). If NAT nucleated heterogeneously on NAD, the percent of NAT drops in each experiment should be independent of the original composition, because once NAD forms the composition of the remaining liquid is fixed. However, Figure 1 shows that experiments with composition higher than 54 wt % HNO_3 yielded <20% NAT drops, while 50 wt % experiments yielded 100% NAT drops. Therefore, we conclude that NAT nucleates homogeneously.

Figure 5 is a plot of ΔG_{act}, calculated with eq 5, as a function of T for both NAD and NAT. This figure shows that the nucleation activation energy for NAT is slightly higher than for NAD in the temperature and composition range studied. ΔG_{act} for NAT, calculated from our results and the results of Bertram and Sloan,[19] is plotted as a function of S_{NAT} in Figure 7; since all the points fall on a straight line, as was the case for NAD, we have performed a linear regression with the following results:

$$\Delta G_{act} = (30.9 \pm 0.3) - (0.139 \pm 0.004) S_{NAT} \quad (10)$$

($r = 0.995$ for the linear regression). This equation is valid for the interval $50 < S_{NAT} < 110$. J_{NAT} can also be calculated for temperatures from 160 to 180 K and concentrations between 43 and 54 wt % HNO_3 using the following equations,

$$\ln J_{NAT} = D(0) + D(1)T + D(2)T^2 + D(3)T^3 + D(4)T^4 \quad (11)$$

$$D(i) = E_i(0) + E_i(1)w + E_i(2)w^2 + E_i(3)w^3 + E_i(4)w^4 \quad (12)$$

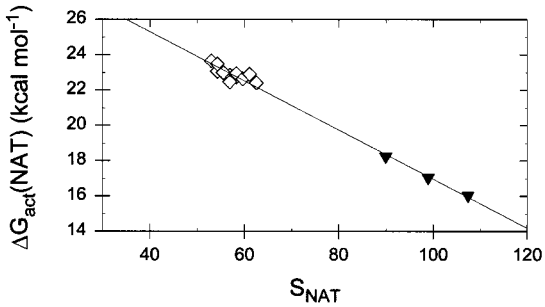

Figure 7. Nucleation activation energy of NAT as a function of the saturation ratio with respect to NAT: (◇) 54 wt % HNO_3, (▼) 53.7 wt % HNO_3.[19] The line was calculated using eq 10.

where w is the concentration of nitric acid in wt % and coefficients $E_i(j)$ are given in Table 3. The maximum difference in J_{NAT} if eqs 11 and 12 are used instead of equations 2 and 10 is 3%. In this case, we only have data for one composition (54 wt % HNO_3), and we have to assume that we can extrapolate these results to other concentrations (similar to the NAD case).

It has been assumed that NAD has a lower nucleation energy barrier than NAT and, hence, that it nucleates more readily;[14] however, this is not necessarily true for all conditions. Comparing Figures 3 and 4, it can be seen that J_{NAD} and J_{NAT} are very similar for 54 wt % HNO_3 solutions at ~180 K; however, at lower temperatures, J_{NAT} is higher. In solutions with composition of 50 wt %, J_{NAD} can become negligible while J_{NAT} still has relatively high values.

Bertram et al.[13] speculated that NAT can form only after NAD nucleates. Their conclusion was based on the fact that the freezing temperature of submicron drops with different compositions (including 53.7 wt % HNO_3) correlated well with S_{NAD}, even when they observed NAT in the most dilute drops. In fact, when ΔG_{act}(NAT) (experimental data in Figure 7) is plotted against S_{NAD}, it follows eq 7 (line in Figure 6), indicating that the results of Bertam et al.[13] agree with ours. However, we think that the correlation between the NAT freezing temperature and S_{NAD} is a coincidence resulting from the similar nucleation rates of NAT and NAD at 53.7 wt %. As discussed above, in our experiments NAT did not nucleate heterogeneously from NAD previously formed.

Barton et al.[26] studied the freezing of approximately 53.7 wt % HNO_3 aerosols with an IR spectrometer and they always observed NAD before NAT appeared, concluding also that NAT forms heterogeneously on NAD, rather than homogeneously. A possible explanation is that the drops in their experiments were slightly more concentrated than they assumed; if this is the case, their results would agree with our conclusions.

As shown in Figure 1, a few NAT drops are observed in the 57 and 60 wt % HNO_3 experiments. We believe that in these

drops NAT nucleates heterogeneously on previously formed NAD, because J_{NAT} is much smaller than J_{NAD}. Furthermore, once NAD is present, the concentration of the remaining solution becomes too dilute to allow the homogeneous nucleation of NAT (for example, at 183 K, NAD is in equilibrium with a 35 wt % solution). NAT is observed only when $T_{min} < \sim 183$ K, which suggests that NAD promotes NAT nucleation below this temperature. We did not observe NAT in any of the 64 wt % HNO_3 drops (not even if the minimum temperature was 173 K), because this composition is slightly higher than the stoichiometric one (63.4 wt % HNO_3). Thus, once NAD forms, the remaining liquid becomes even more concentrated (for example, >80 wt % HNO_3 at 183 K) and NAT is no longer stable.

Implications for Polar Stratospheric Clouds. Stratospheric aerosols contain nitric acid and sulfuric acid. There is experimental evidence that H_2SO_4 decreases the freezing temperature of nitric acid solutions and emulsions.[7,9] This behavior is probably the result of two effects: on one hand, sulfuric acid lowers the saturation ratio of the nitric acid solution with respect to the nitric acid hydrates; on the other hand, it hinders the diffusion of nitric acid molecules. We have shown above that the nucleation rate of NAT and NAD strongly depends on the saturation ratio of the liquid; in addition, the diffusion activation energy for nucleation in binary nitric acid solutions is negligible at stratospheric temperatures. Furthermore, the concentration of sulfuric acid in liquid PSCs is relatively small. Thus, we can assume that the effect of sulfuric acid on the diffusion of nitric acid molecules is small, and hence, the nucleation rates of the nitric acid hydrates in liquid stratospheric aerosols can be estimated using the parametrizations described in the previous sections. We also assume that our experimental data can be extrapolated to saturation ratios beyond the interval in which measurements were carried out. It will be necessary to perform experiments at lower saturation ratios to confirm the conclusions below regarding freezing stratospheric drops in equilibrium with the gas phase. For nonequilibrium aerosol, no extrapolation is necessary.

We have calculated the saturation ratio with respect to NAD and NAT of liquid stratospheric aerosols in equilibrium with the gas phase under typical stratospheric conditions (5 ppm H_2O, 10 ppb HNO_3, and 0.5 ppb H_2SO_4 at 50 mbar). At ~191 K, maximum saturation ratios are attained: $S_{NAT} = 24$ and $S_{NAD} = 5$. According to our experimental results, these values of S_{NAT} and S_{NAD} correspond to nucleation rates, J_{NAD} and J_{NAT}, between 10^4 and 10^5 cm^{-3} s^{-1}. In order for 1% of the drops in a cloud with 1 μm diameter aerosols to freeze on a time scale between 1 day and 1 week, the value of J must lie between 3×10^4 and 2×10^5 cm^{-3} s^{-1}. Hence, the results presented in this work suggest that, if the temperature of the stratosphere remains below the freezing temperature of NAD or NAT for more than 1 day, the largest particles in a liquid PSC might freeze homogeneously.

Field measurements indicate the existence of polar stratospheric clouds composed of external mixtures of liquid and solid particles.[27,28] Larsen et al.[29] found that solid clouds form after long periods, with duration of at least 1−2 days, at temperatures below T_{NAT}, and possibly accompanied by slow, synoptic temperature fluctuations. The observations suggest that homogeneous nucleation of some liquid PSC particles does take place, as explained above.

It has been suggested that denitrification in the stratosphere occurs when nitric acid condenses on solid ice particles, which grow large enough to fall to lower altitudes and cause a permanent removal of NO_x.[30−32] This mechanism is very likely to happen in the Antarctic vortex, since the temperature often drops below the ice frost point. Over the Arctic, where ice PSCs are less prevalent, a more likely mechanism for denitrification consists of freezing of only a small fraction of the liquid particles, as suggested by our experimental results, followed by efficient transfer of nitric acid and water vapor to the solid particles, and the subsequent growth and transport by gravity to lower altitudes. In fact Tabazadeh et al.[33] recently performed PSC statistics for selected periods including two Arctic winters: they suggested that, for crystallization and growth of NAT or NAD clouds, the temperature should remain below the condensation temperature of the solid for 7 or 4 days, respectively. Furthermore, they suggested that ice formation is not a requirement for these solid PSCs to form.

Meilinger et al.[10] and Tsias et al.[11] proposed that under certain conditions caused by mountain lee waves, the smaller drops in a PSC are held at ~190 K for 1 min, and thus, can attain concentrations of 52−58 wt % HNO_3 and <0.1 wt % H_2SO_4. They suggested that those small "nonequilibrium" drops could freeze. In order for this mechanism to take place, J should be on the order of 10^9 cm^{-3} s^{-1}. Figure 3 shows that for 54−57 wt % HNO_3 at 190 K, the NAD nucleation rate have values between 10^5 and 10^7 cm^{-3} s^{-1} (J_{NAT} is even lower, as Figure 4 shows). The effect of H_2SO_4, if any, will be to decrease the nucleation rate further. Furthermore, the required nucleation rate is only attained below 180 K, which is not often reached in the stratosphere. Hence, the mechanism proposed by Meilinger et al.[10] and Tsias et al.[11] is unlikely to take place in the stratosphere, unless the nonequilibrium conditions cause the composition of the drops to be even more concentrated (~64 wt %), or unless the temperatures reached are even lower than suggested (~180 K).

Conclusions

We have measured the nucleation rates of nitric acid dihydrate and trihydrate in concentrated binary nitric acid solutions and parametrized the results with simple equations to calculate the nucleation rate of NAD and NAT at different compositions and temperatures. J_{NAD} and J_{NAT} are found to depend strongly on the saturation ratio of the liquid with respect to the solid. NAD or NAT can preferentially nucleate in binary nitric acid solutions, depending on the temperature and the composition of the liquid. Furthermore, it appears that NAT can nucleate heterogeneously on the surface of NAD at temperatures below 183 K.

Our results suggest that a small fraction of the liquid drops in a PSC can freeze homogeneously if the stratospheric temperature remains near 190 K for more than a day. This mechanism would result in the formation of mixed liquid−solid clouds, which could be the precursors for denitrification of the stratosphere. Nonequilibrium quasi-binary nitric acid solutions formed in mountain lee waves survive for too short a time interval to freeze in the stratosphere unless the temperature drops below 180 K, which is very unlikely.

Acknowledgment. We thank Allan Bertram and Azadeh Tabazadeh for helpful discussions. The research presented in this article is supported by a grant from NASA's Atmospheric Effects of Aircraft Program and Upper Atmospheric Research Program. D.S. acknowledges support from DGAPA at Universidad Nacional Autónoma de México.

References and Notes

(1) Peter, T. *Annu. Rev. Phys. Chem.* **1997**, *48*, 785−822.

(2) Toon, O. B.; Browell, E. V.; Kinne, S.; Jordan, J. *Geophys. Res. Lett.* **1990**, *17*, 393−396.

(3) Browell, E. V.; Butler, C. F.; Ismail, S.; Robinette, P. A.; Carter, A. F.; Higdon, N. S.; Toon, O. B.; Shoeberl, M. R.; Tuck, A. F. *Geophys. Res. Lett.* **1990**, *17*, 385−388.

(4) Molina, M. J.; Zhang, R.; Wooldridge, P. J.; McMahon, J. R.; Kim, J. E.; Chang, H. Y.; Beyer, K. D. *Science* **1993**, *261*, 1418−1423.

(5) Carslaw, K. S.; Luo, B. P.; Clegg, S. L.; Peter, T.; Brimblecombe, P.; Crutzen, P. J. *Geophys. Res. Lett.* **1994**, *21*, 2479−2482.

(6) Tabazadeh, A.; Turco, R. P.; Jacobson, M. Z. *J. Geophys. Res.* 1994, *99*, 12897−12914.

(7) Koop, T.; Luo, B.; Biermann, U. M.; Crutzen, P. J.; Peter, T. *J. Phys. Chem.* **1997**, *A101*, 1117−1133.

(8) Anthony, S. E.; Onasch, T. B.; Tisdale, R. T.; Disselkamp, R. S.; Tolbert, M. A.; Wilson, J. C. *J. Geophys. Res.* **1997**, *102*, 10, 777−10, 784.

(9) Chang, H.-Y. A.; Koop, T.; Molina, L. T.; Molina, M. J. *J. Phys. Chem.* **1999**, *A103*, 2673−2679.

(10) Meilinger, S. K.; Koop, T.; Luo, B. P.; Huthwelker, T.; Carslaw, K. S.; Krieger, U.; Crutzen, P. J.; Peter, T. *Geophys. Res. Lett.* **1995**, *22*, 3031−3034.

(11) Tsias, A.; Prenni, A. J.; Carslaw, K. S.; Onasch, T. P.; Luo, B. P.; Tolbert, M. A.; Peter, T. *Geophys. Res. Lett.* **1997**, *24*, 2303−2306.

(12) Prenni, A. J.; Onasch, T. B.; Tisdale, R. T.; Siefert, R. L.; Tolbert, M. A. *J. Geophys. Res.* **1998**, *103*, 28, 439−28, 450.

(13) Bertram, A. K.; Dickens, D. D.; Sloan, J. J. *J. Geophys. Res.* 2000, in press.

(14) Worsnop, D. R.; Fox, L. E.; Zahniser, M. S.; Wofsy, S. C. *Science* **1993**, *259*, 71−74.

(15) Koop, T.; Ng, H. P.; Molina, L. T.; Molina, M. J. *J. Phys. Chem.* **1998**, *A102*, 8924−8931.

(16) Martin, S. T.; Salcedo, D.; Molina, L. T.; Molina, M. J. *J. Phys. Chem.* **1997**, *101*, 5307−5313.

(17) Salcedo, D.; Molina, L. T.; Molina, M. J. *Geophys. Res. Lett.* **2000**, *27*, 193−196.

(18) Bertram, A. K.; Sloan, J. J. *J. Geophys. Res.* **1998**, *103*, 3553−3561.

(19) Bertram, A. K.; Sloan, J. J. *J. Geophys. Res.* **1998**, *103*, 13, 261−13, 265.

(20) Tisdale, R. T.; Middlebrook, A. M.; Prenni, A. J.; Tolbert, M. A. *J. Phys. Chem.* **1997**, *A101*, 2112−2119.

(21) Kelton, K. F. Crystal nucleation in liquids and glasses. In *Solid State Physics. Advances in Research and Applications*; Ehrenreich, H., Turnbull, D., Eds.; Academic Press Inc.: New York, 1991; Vol. 45, pp 75−177.

(22) Carslaw, K. S.; Clegg, S. L.; Brimblecombe, P. *J. Phys. Chem.* **1995**, *99*, 11, 557−11, 574.

(23) Massucci, M.; Clegg, S. L.; Brimblecombe, P. *J. Phys. Chem.* **1999**, *A103*, 4209−4226.

(24) Tabazadeh, A.; Toon, O. B.; Jensen, E. J. *Geophys. Res. Lett.* **1997**, *24*, 2007−2010.

(25) Pruppacher, H. R.; Klett, J. D. *Microphysics of Clouds and Precipitation*, 2nd ed.; Kluwer Academic Publishers: Netherlands, 1997.

(26) Barton, N.; Rowland, B.; Devlin, J. P. *J. Phys. Chem.* **1993**, *97*, 5848−5851.

(27) Shibata, T.; Shiraishi, K.; Adachi, H.; Iwasaka, Y.; Fujiwara, M. *J. Geophys. Res.* **1999**, *104*, 21603-21611.

(28) Gobbi, G. P.; Donfrancesco, G. D.; Adriani, A. *J. Geophys. Res.* **1998**, *103*, 10, 859−10, 873.

(29) Larsen, N.; Knudsen, B. M.; Rosen, J. M.; Kjome, N. T.; Neuber, R.; Kyrö, E. *J. Geophys. Res.* **1997**, *102*, 23, 505−23, 517.

(30) Wofsy, S. C.; Salawitch, R. J.; Yatteau, J. H.; McElroy, M. B.; Gandrud, B. W.; Dye, J. E.; Baumgardner, D. *Geophys. Res. Lett.* **1990**, *17*, 449−452.

(31) Peter, T.; Müller, R.; Crutzen, P. J.; Deshler, T. *Geophys. Res. Lett.* **1994**, *21*, 1331−1334.

(32) Biermann, U. M.; Presper, T.; Koop, T.; Moessinger, J.; Crutzen, P. J.; Peter, T. *Geophys. Res. Lett.* **1996**, *23*, 1693−1696.

(33) Tabazadeh, A.; Santee M. L.; Danilin, M. Y.; Pumphrey, H. C.; Newman, P. A.; Hamill, P. J.; Mergenthaler, J. L. *Science* **2000**, *288*, 1407−1411.